Computational rules for chemotaxis in the nematode *C. elegans*

Thomas C. Ferrée and Shawn R. Lockery
Institute of Neuroscience
University of Oregon
Eugene, Oregon 97403

February 10, 2001

Abstract

We derive a linear neural network model of the chemotaxis control circuit in the nematode *Caenorhabditis elegans*, and demonstrate that this model is capable of producing nematode-like chemotaxis. By expanding the analytic solution for the network output in time-derivatives of the network input, we extract simple computational rules which reveal how the model network controls chemotaxis. Based on these rules we find that optimized linear networks typically control chemotaxis by computing the first time-derivative of the chemical concentration, and modulating the body turning rate in response to this derivative. We argue that this is consistent with behavioral studies, and a plausible mechanism for at least one component of chemotaxis in real nematodes.

Journal of Computational Neuroscience 6: 263-277 (1999).

1 Introduction

To survive and reproduce, an animal must be able to orient itself to external cues in the environment. The mechanisms of orientation in single-celled organisms, such as *Escherichia Coli* (Berg and Brown, 1972) and *Paramecium* (Van Houten, 1978), are reasonably well understood. Much less is known about the mechanisms of orientation in animals with a nervous system, however, because of the large number of cells involved and the relative complexity of the orientation movements themselves.

The nematode *Caenorhabditis elegans* is an excellent experimental system for studying the neural control of orientation, for several reasons. First, *C. elegans* is a free-living soil nematode that uses chemotaxis, oriented movement in response to a chemical gradient, to locate pockets of bacteria, its food source. Thus, it has evolved a robust form of spatial orientation that is easy to study in the laboratory (Ward, 1973). Second, *C. elegans* has a compact nervous system of 302 identified neurons whose connectivity has been mapped virtually completely (White *et al.*, 1986). This information, together with laser ablations of chemosensory neurons and their follower neurons (Bargmann and Horvitz, 1991; C. Bargmann, personal communication), has provided a candidate neural network for chemotaxis in *C. elegans*. Finally, it has recently become possible to make whole-cell patch-clamp recordings from identified *C. elegans* neurons (Goodman *et al.*, 1998). These recordings, together with the anatomical data, present the opportunity to make anatomically and physiologically detailed models of the *C. elegans* chemotaxis circuit, with the aim of understanding how this circuit produces oriented movement.

In chemotaxis assays, in which nematodes move with little slipping on a flat agar surface, observation of nematode locomotion suggests it consists of a series of "runs" and "tumbles" (Rutherford and Croll, 1979), by analogy to bacterial chemotaxis (Berg and Brown, 1972). During runs, the nematode propels itself across the surface sinusoidally by making a traveling wave of dorsal-ventral contractions along the body. During tumbles, the nematode makes sharp turns, or reverses then resumes forward movement in a new direction. It has been shown that *E. coli* modulates the frequency of tumbles to move up a chemical gradient (Berg and Brown, 1972). It is not yet known whether nematodes modulate aspects of runs, or tumbles, or both to direct their movement during chemotaxis. As a first step in understanding the neural mechanisms of chemotaxis in *C. elegans*, we explored orientation strategies that pertain solely to runs.

In order to perform chemotaxis, the nematode must be able assess the chemical gradient $\vec{\nabla}C$. Previous behavioral studies eliminate several obvious mechanisms. *C. elegans* has bilateral pairs of chemosensory organs at the tip of the head (amphids) and at the tail (phasmids). Mutations which block the function of the organs at the tail, however, do not significantly reduce chemotaxis ability (Ward, 1973), suggesting that *C. elegans* can assess the gradient using head sensory organs alone. The possibility that the nematode compares the concentration between left and right amphids is ruled out by the fact that they are too close together for there to be a detectable concentration difference between them (Ward, 1978). Furthermore, *C. elegans* normally moves on its side, which places the amphids orthogonal to the gradient (Ward, 1978). Thus it is likely that the amphids act as a

single sense organ, such that *C. elegans* samples the chemical concentration at a single point in space. In order to perform chemotaxis, therefore, it must assess the gradient by computing the temporal derivative of concentration as it moves through the chemical environment. Such a mechanism has been established in *E. coli* (Berg and Brown, 1972) and *Paramecium* (Van Houten, 1978), and has been suggested to play a role in *C. elegans* chemotaxis (Dusenbery, 1980).

What is the behavioral strategy for chemotaxis in *C. elegans*? At present the most likely possibility is that the nematode attempts to keep its head pointed up the gradient. The best evidence for this follows from chemotaxis assays using the so-called bent-head mutant (*vab*-10) in which the tip of the head sits at an angle to the rest of the body and tends to drive the nematode off course. The key observation is that *vab*-10 animals attempt to keep the tip of the head, rather than the whole body, pointed up the gradient (Ward, 1973). It is not yet known whether nematodes assess the gradient during the dorsal-ventral head sweeps associated with ordinary sinusoidal locomotion (Ward, 1973), or simply as the nematode moves forward through the environment. In this study, we considered the latter by restricting our attention to a model of the nematode which reflects only on the net forward movement of its body.

The set of orientation strategies available to the neural network for chemotaxis in *C. elegans* is defined by the intrinsic electrical properties of individual neurons and their synaptic connections. Electrophysiological recordings indicate that many neurons in *C. elegans* do not fire all-or-none action potentials (Goodman *et al.*, 1998). Instead, neural signals appear to be encoded by graded electrical potentials. The biological network for chemotaxis in *C. elegans* is likely to be nonlinear in at least two respects. First, the I-V curves for individual neurons, although monotonic, are nonlinear functions of voltage (Goodman *et al.*, 1998). Second, recordings from the nematode *Ascaris suum* show that postsynaptic voltage is a sigmoidal function of presynaptic voltage. Earlier work has shown that small networks of graded-potential neurons with nonlinear synaptic transfer functions are capable of controlling chemotaxis in computer simulations of *C. elegans* (Ferrée *et al.*, 1997). Whether or not these nonlinearities are essential for *C. elegans* chemotaxis remains an important open question.

When seeking to understand a nonlinear system, it is often helpful to study the corresponding linear system first. If the system is linearized appropriately, it may approximate the behavior of the nonlinear system in the domain of interest. In the context of nematode chemotaxis this immediately raises several questions. First, in what output variables might nematode chemotaxis be viewed as linear? Is the two-dimensional spatial trajectory of the nematode a linear function of the input, or is the relevant linear output variable some other quantity, such as the turning rate? Second, what is the appropriate linearization of the nonlinear system? About what point, and over what domain, might the nematode chemotaxis circuit be considered approximately linear? Third, is a linear network sufficient for nematode-like chemotaxis? Fourth, since linear systems of equations are analytically soluble, what insights can be gained about the computational algorithms by which linear networks control chemotaxis?

To answer these questions, we first constructed an idealized mathematical model of the steering mechanism of the nematode body. We then derived a neural network model of the chemotaxis control circuit based on graded-potential neurons and linearized its dependence on voltage. Synaptic connection strengths and other parameters in the model network were adjusted by a numerical optimization procedure to elicit chemotaxis on the spatial and temporal scales of the real animal. We found that small linear networks of graded-potential neurons are capable of controlling nematode-like chemotaxis. Analysis of the model using techniques in linear systems theory revealed the simple computational rules performed implicitly by the network to control chemotaxis. These results define two distinct computational strategies for chemotaxis by linear networks, and improve our understanding of how the nematode nervous system might generate chemotaxis behavior.

2 Model of nematode body

In order to model a behavior like chemotaxis in the nematode, we must consider not only the anatomy and physiology of the chemotaxis control circuit, but also the mechanics of the nematode body. Nematode locomotion on a flat surface has been described in detail by Niebur and Erdös (1991; 1993). They derived and solved the relevant Newtonian force equations describing how muscle tension, elastic and hydrostatic forces within the body, and friction against the substrate combine to generate undulatory movement. Unfortunately, such a thorough treatment is computationally intensive, as they point out. Instead we derived a simplified model of the nematode body which captures the essential features of nematode movement pertinent to chemotaxis on a flat surface.

2.1 Movement on a planar surface

Figure 1a shows a model of the nematode body. The body wall muscles which control locomotion are segmented, with approximately a dozen segments arranged sequentially along the length of the body (Waterston, 1988). In sinusoidal locomotion, if the animal moves without slipping, then each body segment simply follows the one anterior to it. Our nematode body model focuses, therefore, only on the movement of the head segment, since this segment controls the direction of locomotion. We assigned a velocity vector $\vec{v}$ to the head segment, with components

$$\begin{aligned} \frac{dx}{dt} &= v \cos\theta \\ \frac{dy}{dt} &= v \sin\theta \end{aligned} \tag{2.1}$$

where v is the speed, and θ is the direction of movement. During runs nematodes move forward at approximately constant speed (Pierce and Lockery, unpublished), thus $\theta(t)$ is the

only variable through which the network controls the trajectory $(x(t), y(t))$.

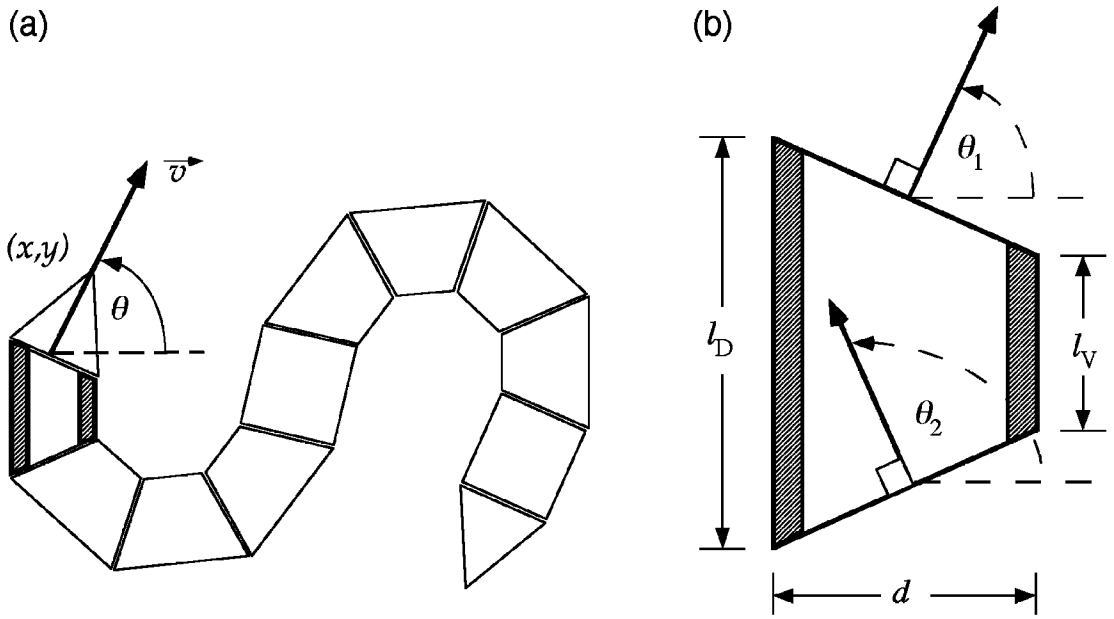

Figure 1: Segmented model of the nematode body. (a) The tip of the nose is located at the point (x, y). Its movement is described by a velocity vector $\vec{v}$, defined by speed $v = 0.022$ cm/s and direction θ. (b) Expanded view of the neck segment. Shaded bands represent dorsal (D) and ventral (V) neck muscles, with lengths l_{D} and l_{V}.

2.2 Geometrical determination of turning rate

Figure 1b shows a detailed geometrical view of the neck segment. Since the body model moves without slipping, the boundary of each segment assumes the position held by its anterior neighbor at a slightly earlier time. If L is the body length and N is the total number of body segments, then this delay is $\delta t \simeq L/Nv$. For $L = 0.1$ cm, $v = 0.022$ cm/s and $N = 12$, we have $\delta t \simeq 0.38$ s, roughly an order of magnitude smaller than the shortest relevant behavioral time scale, the head-sweep period: $T_{\mathrm{head}} = 4.2$ s (Pierce and Lockery, unpublished). Thus it is sensible to think of δt as a positive infinitesimal for the purpose of describing continuous movement of the body. Defining the neck angle $\alpha(t) \equiv \theta_1(t) - \theta_2(t)$ leads to

$$\begin{aligned} \alpha(t) &= \theta_1(t) - \theta_1(t - \delta t) \\ &\simeq \frac{d\theta}{dt}\,\delta t \end{aligned} \tag{2.2}$$

where in the first line we used $\theta_2(t) = \theta_1(t - \delta t)$, and the second line is based on a backward-Euler algorithm for θ_1, and the fact that $\theta = \theta_1$. Equation (2.2) establishes the intuitive result that the neck angle $\alpha(t)$ determines the rate of turning $d\theta/dt$.

2.3 Motor neuron control of turning rate

Figure 1b relates the neck angle $\alpha(t)$ geometrically to the relative voltage of dorsal (D) and ventral (V) motor neurons, as follows. Due to internal hydrostatic pressure, nematodes maintain nearly constant volume during movement. To approximate this constraint, we assumed that the geometry of each segment obeys $(l_{\rm D} - l_0) = -(l_{\rm V} - l_0)$, where $l_0 = L/N$ is the equilibrium length of a relaxed segment. For small neck angles α, this gives $\alpha \simeq (l_{\rm V} - l_{\rm D})/d$, where d is the body diameter. Assuming that *C. elegans* muscles develop tension independent of length (Toida *et al.*, 1975), and that the elastic forces in the body act linearly over the relevant range, then $T_{\rm D} - T_{\rm V} \simeq k \cdot (l_{\rm V} - l_{\rm D})$, where $T_{\rm D}$ and $T_{\rm V}$ are tensions in dorsal and ventral neck muscles, and k is an effective spring constant. Assuming further that the tension in each muscle is proportional to the voltage of its corresponding motor neuron, and that nematode muscles respond quickly to changes in motor neuron voltages, then $T_{\rm D} - T_{\rm V} \simeq \xi \cdot (V_{\rm D} - V_{\rm V})$, where $V_{\rm D}$ and $V_{\rm V}$ are voltages of dorsal and ventral motor neurons, and ξ is a positive constant. Putting all this together leads to

$$\frac{d\theta}{dt} = \gamma \left(V_{\rm D} - V_{\rm V} \right) \tag{2.3}$$

where $\gamma = (Nv/L) \cdot (\xi/kd)$ was included in the optimization as an unknown model parameter.

As described above, during runs the nematode moves along an approximately sinusoidal trajectory, with its instantaneous direction of movement $\vec{v}(t)$ controlled by the bend in the neck $\alpha(t)$. This implies that the voltages of the motor neurons controlling the bend in the neck oscillate in time, and that this oscillation, and in particular the sweeping movements of the head it entails, may be necessary for nematode chemotaxis. Although early work on *C. elegans* chemotaxis suggested that head sweeps may be involved in chemotaxis (Ward, 1973), recent behavioral evidence suggests that the circuit which produces chemotaxis is distinct from the circuit which produces ordinary sinusoidal locomotion. Studies of mutant and laser ablated animals show that animals severely defective in sinusoidal locomotion can nevertheless chemotax accurately (C. Bargmann, personal communication; Rogalski *et al.* 1993; Ward, 1978; Waterston *et al.* 1980). Conversely, animals severely defective in chemotaxis have normal locomotion (Dusenbery, 1976; Lewis and Hodgkin, 1977; S. E. Owens, J. T. Pierce and S. R. Lockery, unpublished). Thus it seems likely that at least one of the mechanisms for chemotaxis in *C. elegans* is independent of head sweeps and relies, therefore, on forward movement alone. To search for a plausible neuronal implementation of such mechanisms, we studied a simplified model which reflects only the net forward movement of the body. During runs, an average velocity vector $\langle \vec{v}(t) \rangle$ can be defined by averaging the instantaneous velocity vector $\vec{v}(t)$ over a single oscillation of the head. This allows a formal separation of changes in chemosensory input due to average forward movement of the body and those due to lateral movement of the head. In what follows, the notation $\vec{v}$ im-

plicitly refers to the average velocity vector only. Returning to (2.3), note that if V_{D} and V_{V} are constant, then $d\theta/dt$ is constant, and θ increases linearly with t. In this case, Eqns. (2.1) make a circular path, with radius $R = v/(d\theta/dt)$. A special case is when $d\theta/dt = 0$, and θ is constant. In this case, Eqns. (2.1) make a straight line.

3 Neural network model of the chemotaxis circuit

What types of chemotaxis strategies are available to the neural network for chemotaxis in *C. elegans*? To address this question, we derived a biophysically realistic, nonlinear neural network model of the *C. elegans* chemotaxis control circuit. This model is based closely on what it known about *C. elegans* neurophysiology, and loosely on *C. elegans* neuroanatomy, as described below. We then linearized its dependence on voltage to obtain a simplified model amenable to analytic study. Deriving the linear model from a more biologically detailed nonlinear model is valuable because it allows one to interpret the various parameters in the linear model, and to clarify which physiological features remain after linearization.

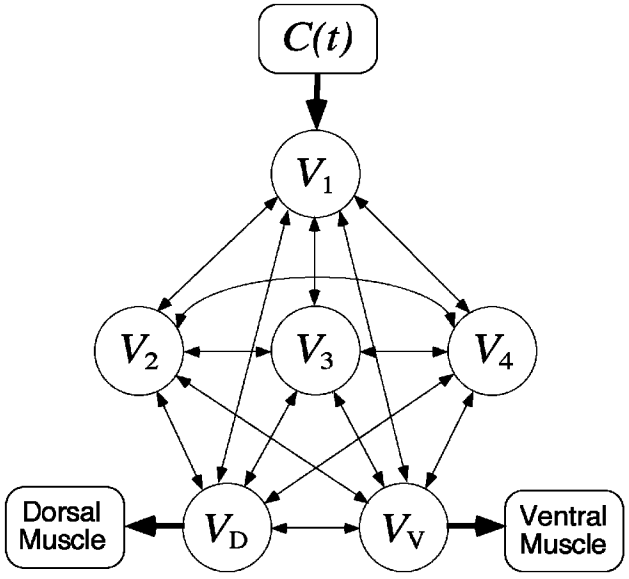

Figure 2: Neural network model of the chemotaxis control circuit of *C. elegans*. The state variable of each neuron (circle) is voltage (V_i). The model contains one chemosensory neuron (V_1), three interneurons ($V_2 - V_4$), and two motor neurons (V_{D}, V_{V}). The chemosensory neuron receives input equal to the chemical concentration $C(t)$ at the tip of the nose, and the motor neurons innervate dorsal (D) and ventral (V) neck muscles.

3.1 Biologically-motivated nonlinear network model

Network architecture. In *C. elegans*, identified neurons can be ablated in intact, living animals using a small laser beam. This technique has revealed which neurons are required

for normal chemotaxis in *C. elegans*. The chemotaxis circuit appears to include four pairs of chemosensory neurons, four pairs of interneurons, and five pairs of motor neurons (Bargmann and Horvitz, 1991; C. Bargmann, personal communication). Anatomical data on the synaptic connections among these neurons (White *et al.*, 1986) reveal chemical synapses making both feedforward and feedback connections, as well as gap junctions. As a first step, we implemented an idealized network model which captures the two main features of the biological circuit (Fig. 2). First, the model network has three distinct types of neurons, including one chemosensory neuron, three interneurons, and two motor neurons. Second, the model network is recurrent, having both feedforward and feedback connections. While the model network certainly does not represent all details of the biological network, it is likely to be adequate for searching for the general types of control strategies which are available to the biological network. Later we will argue that similar strategies are likely to arise from models based more closely on the anatomical data.

Neurons. *C. elegans* neurons are tiny and morphologically simple (White *et al.*, 1986). A typical neuron has a soma 2-3 μm in diameter and just one or two unbranched processes. Electrophysiological recordings indicate that many *C. elegans* neurons are effectively isopotential (Goodman *et al.*, 1998) and can therefore be represented as single electrical compartments. Since these neurons exhibit only graded potentials (Goodman *et al.*, 1998), voltage, rather firing rate, is the appropriate state variable for neural network simulations. In addition, the steady-state *I-V* curves for *C. elegans* neurons are monotonically increasing functions of voltage, and display a broad linear region in the vicinity of the zero-current potential (Goodman *et al.*, 1998). We therefore modeled each cell as a single electrical compartment with passive membrane. Thus the appropriate equation for the voltage V_i of the i^{th} neuron is

$$C_i^{\text{cell}} \frac{dV_i}{dt} = -G_i^{\text{cell}} \cdot \left(V_i - E_i^{\text{cell}}\right) - I_i^{\text{elec}}(\mathbf{V}) - I_i^{\text{chem}}(\mathbf{V}) - I_i^{\text{sens}}(t) \tag{3.1}$$

where C_i^{cell} is the whole-cell capacitance, G_i^{cell} is the effective ohmic conductance associated with the linear region of the *I-V* curve, and E_i^{cell} is the resting potential of an isolated neuron. Here $I_i^{\text{elec}}(\mathbf{V})$ and $I_i^{\text{chem}}(\mathbf{V})$ represent electrical and chemical synaptic currents, $\mathbf{V} = (V_1, ..., V_N)$ is an N-dimensional vector comprised of the voltages of all N neurons in the network, and $I_i^{\text{sens}}(t)$ represents chemosensory input.

Synapses. No data are available yet on synaptic physiology in *C. elegans*. In the larger nematode *Ascaris suum*, however, it was found that chemical synapses release neurotransmitter tonically, and that steady-state postsynaptic voltage is a sigmoidal function of presynaptic voltage (Davis and Stretton, 1989). Assuming chemical synapses in *C. elegans* are similar, we modeled them according to

$$I_i^{\text{chem}}(\mathbf{V}) = \sum_{j=1}^{N} G_{ij}^{\text{chem}} \cdot \sigma\left(\beta_{ij}\ (V_j - \overline{V}_j)\right) \cdot (V_i - E_{ij}) \tag{3.2}$$

where G_{ij}^{chem} is the maximum conductance in cell i due to synaptic connections from cell j, and E_{ij} is the reversal potential for the corresponding postsynaptic current. The postsynaptic conductance in cell i was modeled as a function of presynaptic voltage by the sigmoidal function $\sigma(x) \equiv 1/(1+\exp(-x))$, where $\overline{V}_j$ and β_{ij} are constants which fix the center and steepness of this conductance in (3.2). Assuming that electrical synapses in *C. elegans* are nonrectifying, we modeled them according to

$$I_i^{\text{elec}}(\mathbf{V}) = \sum_{j=1}^{N} G_{ij}^{\text{elec}} \cdot (V_i - V_j) \tag{3.3}$$

where G_{ij}^{elec} is a constant conductance.

Chemosensory input. As described in the Introduction, *C. elegans* chemotaxis most likely requires computation of the time derivative of the chemosensory input. This computation might be performed by the chemotaxis network, or by individual chemosensory neurons, as suggested by Ward (1978). In the absence of physiological data indicating the latter, we made the minimal assumption that the chemosensory neuron V_1 receives an excitatory current proportional to the instantaneous chemical concentration at the tip of the nose:

$$I_i^{\text{sens}}(t) = -\delta_{i1}\ \kappa_{\text{sens}}\ C(t) \tag{3.4}$$

where $C(t) \equiv C(x(t), y(t))$ is the chemical concentration at the tip of the nose, δ_{ij} is the Kronecker delta, and κ_{sens} is a constant parameter.

3.2 Linearization of the network model

As modeled in (3.2), the synaptic current $I_i^{\text{chem}}(\mathbf{V})$ makes the model network nonlinear in voltage. It may be, however, that the basic functioning of the chemotaxis circuit does not rely heavily upon these nonlinearities. To test the hypothesis that small linear networks of graded-potential neurons can control chemotaxis, and to arrive at a simplified model amenable to analytic analysis, we linearized the dependence of (3.2) on voltage.

Any linearization procedure must specify a state of the network, in this case the voltage V_i of each neuron, about which the dynamics will be approximated. In *Ascaris suum*, it has been shown that the resting potential of neurons with tonically active chemical synapses tend to sit near the middle of their voltage-sensitive range for neurotransmitter release (Davis and Stretton, 1989). This implies a fixed point of the network obeying $d\mathbf{V}/dt = 0$, at which each neuron releases transmitter at half its maximum rate. If only chemical synapses are included in the model, this leads to an explicit expression for $\overline{V}_i$:

$$\overline{V}_i = \left[G_i^{\text{cell}} E_i^{\text{cell}} + \frac{1}{2} \sum_{j=1}^{N} G_{ij}^{\text{chem}} E_{ij} \right] \div \left[G_i^{\text{cell}} + \frac{1}{2} \sum_{j=1}^{N} G_{ij}^{\text{chem}} \right] \tag{3.5}$$

If both electrical and chemical synapses are included in the model, the values of the $\overline{V}_i$ must be obtained by matrix inversion, as described by Wicks *et al.* (1996).

To linearize the network, we made a Taylor series expansion of (3.1) about the point $\mathbf{V} = \overline{\mathbf{V}}$, and kept only linear terms. The result can be written

$$\frac{dV_i}{dt} = \sum_{j=1}^{N} A_{ij}\ V_j + b_i + c_i(t) \tag{3.6}$$

where the matrix

$$\begin{aligned} A_{ij} \;\; = \;\; & \frac{-1}{C_i^{\text{cell}}} \left\{ \delta_{ij} \Big[G_i^{\text{cell}} + \sum_{k=1}^{N} G_{ik}^{\text{elec}} + \frac{1}{2} \sum_{k=1}^{N} G_{ik}^{\text{chem}} \Big] \right. \\ & \left. + \Big[-G_{ij}^{\text{elec}} + \frac{1}{4} \beta_{ij} G_{ij}^{\text{chem}} \cdot \big(\overline{V}_i - E_{ij} \big) \Big] \right\} \end{aligned} \tag{3.7}$$

the constant vector

$$b_i = \frac{1}{C_i^{\text{cell}}} \Big[G_i^{\text{cell}} E_i^{\text{cell}} + \frac{1}{2} \sum_{j=1}^{N} G_{ij}^{\text{chem}} E_{ij} + \frac{1}{4} \sum_{j=1}^{N} \beta_{ij} G_{ij}^{\text{chem}} \overline{V}_j \cdot \big(\overline{V}_i - E_{ij} \big) \Big] \tag{3.8}$$

and the time-dependent vector

$$c_i(t) = \delta_{i1} \frac{\kappa_{\text{sens}}}{C_i^{\text{cell}}} C(t) \tag{3.9}$$

We now consider Eqn. (3.6), along with (2.1) and (2.3), to be our model of the nematode. Equation (3.6) comprises a standard linear system of equations, which can be solved analytically. This linear network was derived from (3.1), based on the assumption that the voltage of each neuron remains near the linear region of its I-V curve, and the linear region of its sigmoidal function for neurotransmitter release. Since we want to study arbitrary movement in two dimensions, however, there is no argument which supports linearization of (2.1) in the variable θ. In addition, we want to study chemotaxis in nonlinear chemical environments $C(x, y)$. Hence our model of the nematode is still nonlinear in x, y and θ, and is not analytically soluble, except in very limited special cases (see discussion following (2.3)). As we demonstrate in Section 5, however, analytic solution of (3.6), and analysis of (2.3) and (3.6), is sufficient to understand chemotaxis control in the model.

By linearizing (3.1), we arrived at (3.6). It would be reasonable to ask, therefore, why we did not simply postulate (3.6) in the first place. By deriving the linear model from a biophysically realistic nonlinear model, one can interpret the parameters in (3.6) physiologically. As an example, note that the diagonal elements of A_{ij} differ from G_i^{cell} due to the presence of gap junctions and tonically active chemical synapses. This is relevant because each diagonal element of A_{ij} can be interpreted as the net input conductance G_i^{input} for the i^{th} cell, and the ratio $C_i^{\text{cell}}/G_i^{\text{input}}$ can be viewed as its effective time constant τ_i^{eff}. Thus, our linear model has the feature that τ_i^{eff} is affected by synaptic connections. This arises because our linearization procedure maintains proper dependence on both presynaptic and postsynaptic voltages.

4 Chemotaxis control by a linear neural network

Simulating nematode chemotaxis in this model requires selecting an environment $C(x, y)$ and solving equations (2.1), (2.3) and (3.6) for the state trajectory $S(t) = (x(t), y(t), \theta(t), \mathbf{V}(t))$, beginning from some initial state $S_0 = (x_0, y_0, \theta_0, \mathbf{V}_0)$. In our simulations, these equations were solved numerically using a fourth-order Runge-Kutta integration scheme with $\Delta t = 0.1$ s. The network was optimized by finding model parameters which maximized a fitness function meant to capture the basic features of nematode chemotaxis behavior.

4.1 Network optimization by simulated annealing

The chemotaxis behavior of our model nematode based on (3.6) depends on the set of parameters $\Gamma \equiv (A_{ij}, b_i, \kappa_{\rm sens}/C_1^{\rm cell}, \gamma)$. For simplicity, we optimized the parameters in (3.6) directly, rather than the more numerous parameters in the original model. Each distinct parameter set Γ can be thought of as a different candidate network model for *C. elegans* chemotaxis. The goal of optimization is to find sets Γ which maximize a chemotaxis fitness function, as described below.

To simulate chemotaxis control by a particular network, model nematodes were placed in a simulated chemical environment described by

$$C(x, y) = C_0 \exp\Big[-(x^2 + y^2)/2\lambda^2\Big] \tag{4.1}$$

where $C_0 = 1$ mM and $\lambda = 1.61$ cm. This represents the type of gradient used in standard chemotaxis assays (Ward, 1973). The model nematode was initialized in a state S_0, and Eqns. (2.1), (2.3) and (3.6) were integrated numerically for $T \simeq 5$ minutes. To eliminate transients which are independent of the stimulus, we took $V_i(t_0) = -\sum_{j=1}^{N} (A^{-1})_{ij} b_j$. We then used a simple, simulated-annealing training algorithm (Masters, 1995) to maximize a fitness function F, defined by

$$F = \left\langle \frac{1}{T} \int_0^T C(t)\, dt \right\rangle \tag{4.2}$$

where $C(t) \equiv C(x(t), y(t))$. The brackets denote an average over initial positions (x_0, y_0) and angles θ_0. During training, we typically averaged over 90 initial positions, taking $\sqrt{x_0^2 + y_0^2} = 2$ cm and evenly spaced values of θ_0. As is typical in stochastic network optimization, only local maxima were found, and different maxima had distinct behaviors and chemotaxis strategies. Nevertheless, the computational strategies of networks obtained by this procedure can be grouped into categories according to a simple scheme, as shown in the next section.

4.2 Numerical results: chemotaxis control by the neural network

Figure 3 shows the chemotaxis behavior of real and simulated nematodes. In Fig. 3a, four real nematodes were placed in a petri dish and allowed to move freely for $T = 5$ minutes. After a period of initial wandering, each nematode moved almost directly up the gradient

and dwelled at the peak (Pierce and Lockery, unpublished). Figure 3b shows the chemotaxis behavior of a particular linear network, denoted Γ_1. The model nematode was initialized at four points for which $r_0 = 3$ cm and $\theta_0 = 0$, and moved in its environment for $T = 5$ minutes. After initial transient movements, each initial condition led to oriented movement up the gradient and persistent dwelling at the peak, in good general agreement with the behavior of real nematodes. Similar behavior was seen for nearly any initial condition, provided $r_0 < r_{\text{dish}}$. Similar behavior was also seen for other networks obtained by this optimization procedure (see Table 1).

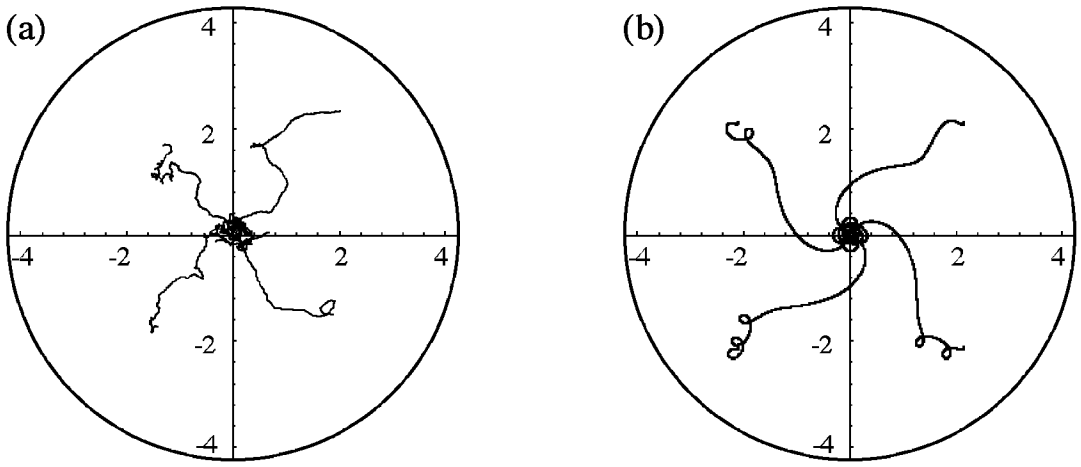

Figure 3: Chemotaxis control by neural networks: (a) biological nematodes, (b) model nematodes controlled by network Γ_1. In both cases, simulation time $T = 5$ minutes. Axes labels are in cm.

5 Extraction of computational rules for chemotaxis

We have shown that the linear network model (3.6) can be optimized to control chemotaxis in a nematode-like physical body. Simple inspection of the parameters Γ does not necessarily lead to an intuitive understanding of how the network functions, however, because the neural architecture and optimization procedure often favor a distributed representation of the control algorithm. To derive an intuitive mathematical expression for this algorithm, we manipulated the analytic solution to (3.6).

5.1 Analytic solution for the linear recurrent network

The solution to (3.6) is derived in standard texts (Boyce and DiPrima, 1977), and is not repeated here. With a convenient choice of initial voltages, $V_i(t_0) = -\sum_{j=1}^{N}(A^{-1})_{ij}b_j$, the solution can be written

$$V_i(t) = \sum_{j=1}^{N} \Big[-(A^{-1})_{ij} b_j + \int_{t_0}^{t} K_{ij}(t-t')\ c_j(t')\ dt' \Big] \tag{5.1}$$

where the components of the matrix kernel K_{ij} are given by

$$K_{ij}(t-t') = \sum_{\alpha=1}^{N} T_{i\alpha} (T^{-1})_{\alpha j} \exp\Big[a_\alpha (t-t') \Big] \tag{5.2}$$

The summation index α represents a sum over *normal modes* of the system. The complex frequencies a_α are the eigenvalues of A_{ij}, and $T_{i\alpha}$ is an $N \times N$ matrix, whose columns are the eigenvectors $\xi_i^{(\alpha)}$ of A_{ij}.[1] This choice of $V_i(t_0)$ is consistent with that used in network simulations based on (3.6).

Inserting (5.1) and (3.9) into (2.3) leads to

$$\frac{d\theta}{dt} = \Omega_{\text{bias}} + \int_{t_0}^{t} k(t-t')\ C(t')\ dt' \tag{5.3}$$

where the constant

$$\Omega_{\text{bias}} \equiv -\gamma \sum_{j=1}^{N} \Big[(A^{-1})_{\text{D}j} - (A^{-1})_{\text{V}j} \Big]\ b_j \tag{5.4}$$

and the scalar kernel

$$k(t-t') \equiv \frac{\gamma \kappa_{\text{sens}}}{C_1^{\text{cell}}} \Big[K_{\text{D1}}(t-t') - K_{\text{V1}}(t-t') \Big] \tag{5.5}$$

The first term in (5.3) represents a constant turning bias. The second term in (5.3) represents the cumulative effect of chemosensory input $C(t')$ on the rate of turning $d\theta/dt$.

5.2 Taylor expansion in time-derivatives of the input

Equation (5.3) produces exactly the same response to chemosensory as the original network (3.6). Figure 4a shows the scalar kernel $k(t-t')$ for the network Γ_1, which generated Fig. 3b. The oscillation arises because some eigenvalues a_α are complex. More importantly, $k(t-t')$ has an exponentially decaying envelope, which originates from the fact that all eigenvalues of A_{ij} have negative real part.[2] The form of the solution written in (5.3) improves our understanding of chemotaxis control by the network only slightly, however, since it requires us to think of a weighted integral of sensory input over the entire history of the system.

To further improve our intuition about chemotaxis control in this model, we expanded (5.3) in time-derivatives of the input. This expansion was motivated by the fact that the

[1] Strictly speaking, (5.2) holds only if the eigenvectors $\xi_i^{(\alpha)}$ of A_{ij} span its space. This was the case for all networks studied here, and is likely to be the case for any network whose matrix A_{ij} is real-valued and found by a stochastic optimization procedure.

[2] This general stability requirement, which must be satisfied by any linear system, is satisfied by all networks discussed here.

kernel $k(t-t')$ decays to zero in only a few seconds, which is very short compared to the time scale $T \sim$ minutes, required for nematode chemotaxis. Consequently, although (5.3) shows that the rate of turning $d\theta/dt$ at time t depends on the entire history of the input $C(t')$, the rapid decay of $k(t-t')$ implies that the integral accumulates contributions from $C(t')$ only for times $t' \lesssim t$. This suggests a Taylor series expansion of $C(t')$ about the time t:

$$C(t') = C(t) + \frac{dC}{dt}\,(t'-t) + \frac{1}{2!}\,\frac{d^2C}{dt^2}\,(t'-t)^2 + \ldots \tag{5.6}$$

The *order* of this expansion is defined as the highest number of time derivatives retained in (5.6).

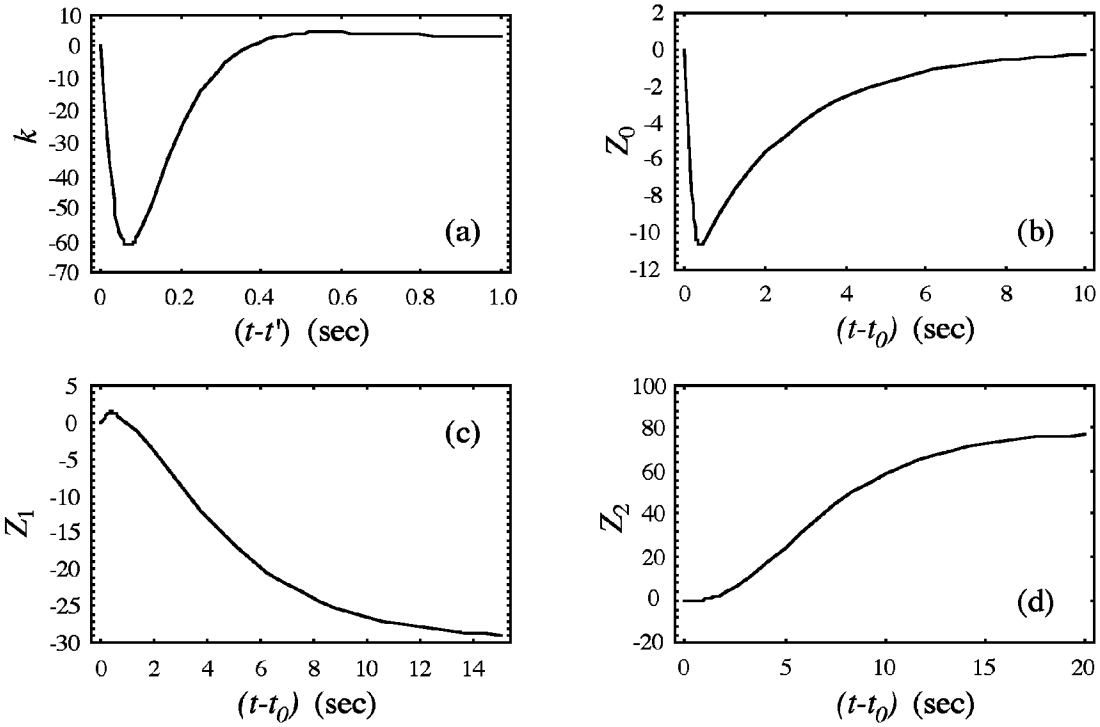

Figure 4: Scalar kernel $k(t-t')$, and transient expansion coefficients $Z_0(t-t_0)$, $Z_1(t-t_0)$, and $Z_2(t-t_0)$ for the network Γ_1.

When (5.6) is inserted into (5.3), the quantities $C(t)$, dC/dt, d^2C/dt^2, etc., can be removed from the integral sign, since they are independent of t'. This yields

$$\frac{d\theta}{dt} = \Omega_{\text{bias}} + Z_0(t-t_0)\;C(t) + Z_1(t-t_0)\,\frac{dC}{dt} + Z_2(t-t_0)\,\frac{d^2C}{dt^2} + \ldots \tag{5.7}$$

where the *transient expansion coefficients* are defined

$$Z_n(t-t_0) \equiv \frac{1}{n!}\int_{t_0}^{t} k(t-t')\,(t'-t)^n\,dt' \tag{5.8}$$

Since $k(t-t')$ is a sum of exponential functions of $(t-t')$, the $Z_n(t-t_0)$ can be computed analytically using the standard integral formula

$$\int x^n \mathrm{e}^{ax} dx = \frac{1}{a} x^n \mathrm{e}^{ax} - \frac{n}{a} \int x^{n-1} \mathrm{e}^{ax} dx \ , \qquad n \geq 1 \tag{5.9}$$

Together with (2.1) and (2.3), (5.7) constitutes a simple rule for chemotaxis control, which relates the body rate of turning $d\theta/dt$, to time derivatives of the chemosensory input $C(t')$. Because the $Z_n(t-t_0)$ are functions of $(t-t_0)$, the expansion (5.7) has transient behavior, e.g., $Z_0(t-t_0)$ is the transient response to a unit step input at time t_0. The time dependence of the $Z_n(t-t_0)$ can be important for reproducing the detailed behavior of some networks, as noted by Ferrée and Lockery (1998).

For the networks studied here, however, (5.7) can be further simplified. The Taylor series expansion (5.6) was motivated by the fact that the scalar kernel $k(t-t')$ decays to zero rapidly compared to the behavioral time scale T. Figures 4b–d show the $Z_n(t-t_0)$ for the kernel $k(t-t')$ in Fig. 4a. Like the kernel $k(t-t')$, each $Z_n(t-t_0)$ approaches its (nonzero) asymptotic value rapidly compared to T, suggesting that only these asymptotic values are relevant to describe the behavior on time scales $\sim T$. Their asymptotic behavior can be isolated by taking the limit $t_0 \to -\infty$ in (5.7), to obtain

$$\frac{d\theta}{dt} = \Omega_{\text{bias}} + z_0 \ C(t) + z_1 \ \frac{dC}{dt} + z_2 \ \frac{d^2C}{dt^2} + \ldots \tag{5.10}$$

where the *constant expansion coefficients* are defined

$$\begin{aligned} z_n &\equiv \lim_{t_0 \to -\infty} Z_n(t-t_0) \\ &= \sum_{\alpha=1}^{N} \frac{r_\alpha}{a_\alpha^{n+1}} \end{aligned} \tag{5.11}$$

where $r_\alpha \equiv -(\gamma \kappa_{\text{sens}}/C_1^{\text{cell}}) \left[T_{\text{D}\alpha} T_{\alpha 1}^{-1} - T_{\text{V}\alpha} T_{\alpha 1}^{-1} \right]$. Like (5.7), (5.10) constitutes a simple rule for chemotaxis control. The difference is that (5.10) lacks transient behavior, which is present in (5.7).

Implementing the computational rule (5.10) requires numerical values for C and its time-derivatives. In our simulations we used the fact that for any point sensor moving at constant speed v in two dimensions, the first derivative is given by

$$\begin{aligned} \frac{dC}{dt} &= \vec{v} \cdot \vec{\nabla} C \\ &= v \left[\cos\theta \ \frac{\partial C}{\partial x} + \sin\theta \ \frac{\partial C}{\partial y} \right] \end{aligned} \tag{5.12}$$

and the second derivative is given by

$$\begin{aligned}\frac{d^2C}{dt^2} &= \frac{d\vec{v}}{dt}\cdot\vec{\nabla}C + \vec{v}\cdot\vec{\nabla}\left(\frac{dC}{dt}\right) \\ &= v\left[-\sin\theta\ \frac{\partial C}{\partial x} + \cos\theta\ \frac{\partial C}{\partial y}\right]\ \frac{d\theta}{dt} \\ &\quad + v^2\left[\cos^2\theta\ \frac{\partial^2 C}{\partial x^2} + 2\cos\theta\ \sin\theta\ \frac{\partial^2 C}{\partial x \partial y} + \sin^2\theta\ \frac{\partial^2 C}{\partial y^2}\right]\end{aligned} \tag{5.13}$$

Note that the first derivative dC/dt has a particularly simple relation to the gradient $\vec{\nabla}C$. This fact will be useful for interpreting our numerical results. When including the second derivative d^2C/dt^2, inserting (5.13) into (5.10) yields an expression with $d\theta/dt$ appearing on *both* sides. Writing $d^2C/dt^2 = \mu(x,y,\theta) + \nu(x,y,\theta)d\theta/dt$ and solving algebraically for $d\theta/dt$ yields $d\theta/dt \simeq [\Omega_{\rm bias} + z_0C(t) + z_1 dC/dt + z_2\mu(x,y,\theta)]/[1 - z_2\nu(x,y,\theta)]$.

Before presenting numerical results, further insight on expansion (5.10) can be gained by combining (5.11), (5.12) and (5.13) for the Gaussian gradient (4.1). Direct substitution leads to the following expressions for the zeroth-order term

$$z_0 C(x,y) = \sum_{\alpha=1}^{N} \frac{r_\alpha}{a_\alpha}\ C(x,y) \tag{5.14}$$

for the first order term

$$z_1 \frac{dC}{dt} = \sum_{\alpha=1}^{N} \frac{r_\alpha}{a_\alpha}\left(\frac{v}{\lambda a_\alpha}\right)\left[-\frac{x}{\lambda}\cos\theta - \frac{y}{\lambda}\sin\theta\right]\ C(x,y) \tag{5.15}$$

and for the second order term

$$\begin{aligned} z_2\frac{d^2C}{dt^2} &= \sum_{\alpha=1}^{N} \frac{r_\alpha}{a_\alpha}\left(\frac{v}{\lambda a_\alpha}\right)^2\left[\left(\frac{x}{\lambda}\sin\theta - \frac{y}{\lambda}\cos\theta\right)\frac{\lambda}{v}\frac{d\theta}{dt}\right. \\ &+ \left.\left(-1 + \frac{x^2}{\lambda^2}\cos^2\theta + \frac{2xy}{\lambda^2}\cos\theta\sin\theta + \frac{y^2}{\lambda^2}\sin^2\theta\right)\right]\ C(x,y) \end{aligned} \tag{5.16}$$

The algebraic form of these expressions suggests that our expansion can alternatively be viewed as a perturbative series in the small parameter $\epsilon_\alpha \equiv v/(\lambda|a_\alpha|)$. Using numerical values for the a_α derived from the linear network in Section 4.2, for example, gives ϵ_α ranging from 0.001 to 0.03. Assuming that the other factors in (5.14)–(5.17) are of order unity, this suggests that the series (5.10) should converge as increasing derivatives of the stimulus are included. In the next section, this result is demonstrated numerically.

We wish to emphasize, however, that the interpretation of (5.10) as a perturbative series in the small parameter ϵ_α is meant here only to be suggestive. A rigorous interpretation of this sort is precluded by the fact that (1) the eigenvalues a_α are in general complex and

this has not been dealt with carefully here, (2) expressions (5.14)–(5.17) are valid only for the Gaussian gradient (4.1), and (3) we have computed terms only through second order in ϵ_α. These expressions are included only to improve one's intuition for the numerical results presented in the next section.

5.3 Numerical results: chemotaxis control by an extracted rule

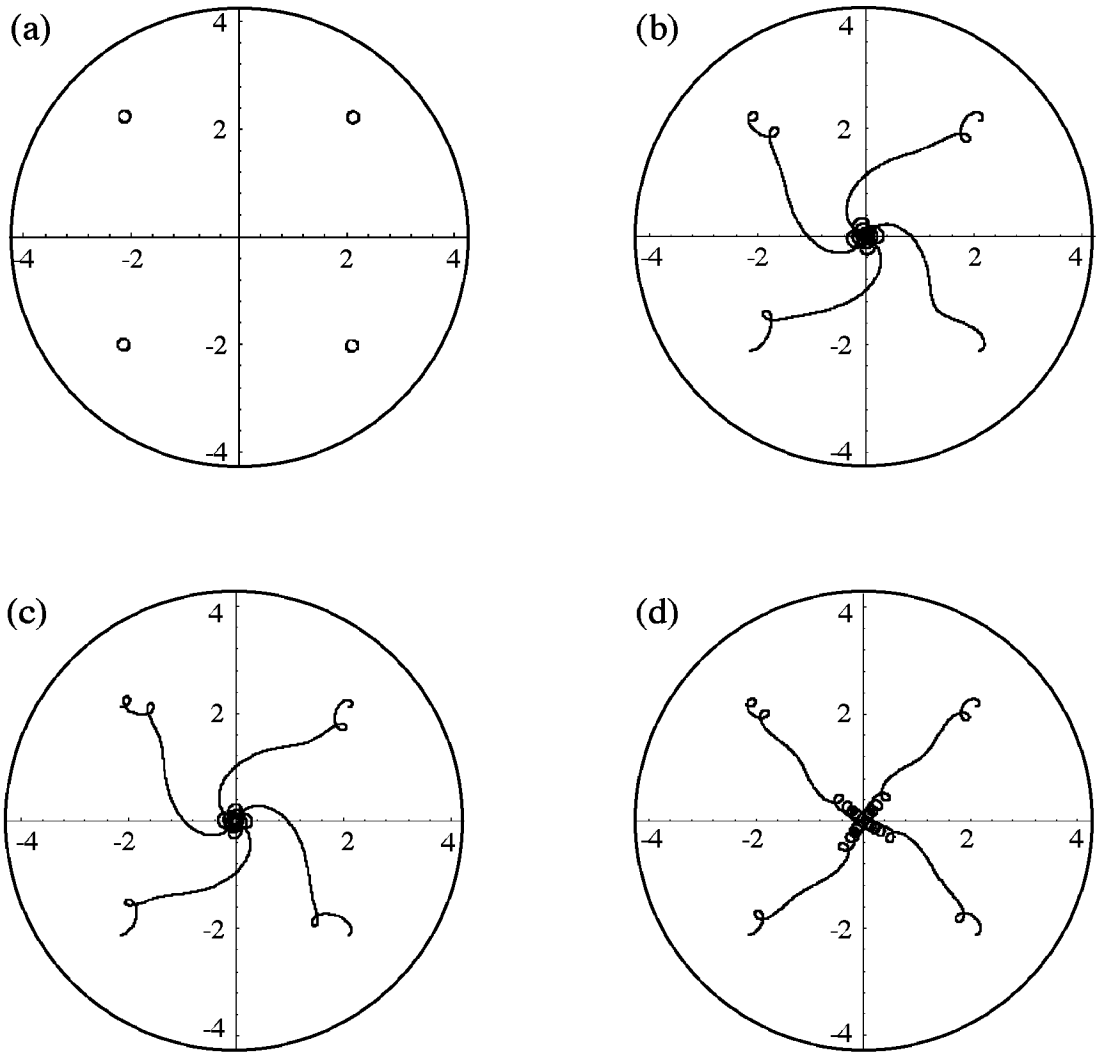

Figure 5: Chemotaxis control by extracted rule (5.10) for network Γ_1: (a) zeroth order, (b) first order, (c) second order, (d) first order, but omitting zeroth-order term. Initial conditions and duration of the simulations were the same as in Fig. 3b.

Figure 5 shows numerical results for the computational rule (5.10). The constant coefficients z_n were computed from network parameters Γ_1, used to generate Fig. 3b. Figure 5a shows the result of keeping terms in (5.10) through zeroth order in (5.10), i.e., Ω_{bias} and z_0.

This rule failed to produce chemotaxis for any initial condition. Longer simulation times showed that a model nematode controlled by this rule moves in an approximate circle, whose center migrates slowly around the origin with fixed radius. Figure 5b shows the result of keeping all terms through first order in (5.10), i.e., $\Omega_{\rm bias}$, z_0 and z_1. This rule also led to oriented movement up the gradient and persistent dwelling near the peak for all initial conditions, and accurately reproduced the tracks generated by the network. Figure 5c shows the result of keeping all terms through second order in (5.10). The tracks generated by this rule were nearly identical to those in Fig. 5b, indicating numerically that (5.10) has effectively converged by first order for this network.

	$\Omega_{\rm bias}(\mathrm{s}^{-1})$	$z_0(\mathrm{mM}^{-1}\mathrm{s}^{-1})$	$z_1(\mathrm{mM}^{-1})$	$z_2(\mathrm{mM}^{-1}\mathrm{s})$
Γ_1	$+0.2182$	-0.0755	-29.34	$+77.86$
Γ_2	-0.2143	-0.1044	$+39.80$	-0.4885
Γ_3	0	-0.5621	$+37.25$	-88.27
Γ_4	0	$+0.4881$	-31.46	$+33.39$

Table 1. Constant turning biases (5.4) and expansion coefficients (5.11), for four representative networks (Γ_1 – Γ_4).

Figure 5d shows the result of keeping only $\Omega_{\rm bias}$ and z_1, and is helpful in understanding the basic mechanism of chemotaxis control by (5.10). This rule led to oriented movement up the gradient, and persistent dwelling near the peak. Compared to Figs. 3b, 5b and 5c, however, dwelling near the peak occurred prematurely. This behavior can be understood quantitatively by referring to the constant expansion coefficients for network Γ_1, shown in Table 1. In Fig. 5d, the rule is of the form $d\theta/dt \simeq \Omega_{\rm bias} + z_1 dC/dt$. Since $\Omega_{\rm bias}$ and z_1 have opposite sign, it is possible to make $d\theta/dt \simeq 0$, provided $dC/dt > 0$. Using (5.12), we find that $d\theta/dt = 0$ when $|\vec{\nabla}C| \simeq -0.34$ mM/cm and $\vec{v}$ is pointed radially inward. For $C(x,y)$ described by (4.1), $|\vec{\nabla}C|$ takes this value at $r \simeq 1.1$ cm and 2.1 cm, and takes approximately this value for a large region of the dish over which oriented movement occurred. Thus oriented movement in Fig. 5d arises from a cancellation between two terms: the first-order term $z_1 dC/dt$, and the constant bias $\Omega_{\rm bias}$. In behavioral terminology, this first-order $z_1 dC/dt$ term represents a strategy called klinotaxis: a change in turning rate in response to the spatial gradient of a stimulus field (Dunn, 1990).

The effect of the zeroth-order term on dwelling near the peak, seen by comparing the tracks in Fig. 5b with those in Fig. 5d, can be understood by noting that z_0 has the same sign as z_1. Near the peak, where $|\vec{\nabla}C| \simeq 0$ makes $dC/dt \simeq 0$, the product $z_0 C$ is largest and so partly compensates for the reduction in the first-order term. This prevents premature dwelling near the peak, seen in Fig. 5d. In behavioral terminology, this zeroth-order $z_0 C$ term represents a strategy called klinokinesis: a change in turning rate in response to the scalar value of a stimulus field (Dunn, 1990). Thus network Γ_1 uses primarily klinotaxis, but also klinokinesis, to produce the behavior seen in Fig. 3b.

Similar results were obtained from other results of the optimization algorithm. As another

example, consider constant expansion coefficients for network Γ_2, shown in Table 1. Since $\Omega_{\text{bias}} < 0$, this model has a rightward turning bias. As for Γ_1, z_0 is small, and the sign of z_1 is opposite that of Ω_{bias}. The primary behavior is again klinotaxis, but for Γ_2, the zeroth-order (klinokinesis) term has the opposite effect. Unlike Γ_1, the sign of z_0 is opposite z_1, and has the effect of tightening the tracks near the peak. Consequently, tracks generated by the network Γ_2, and its corresponding first-order rule, markedly resemble those in Fig. 5d. Likewise, omitting the zeroth-order term from Γ_2 produces tracks that resemble those in Figs. 3b, 5b and 5c.

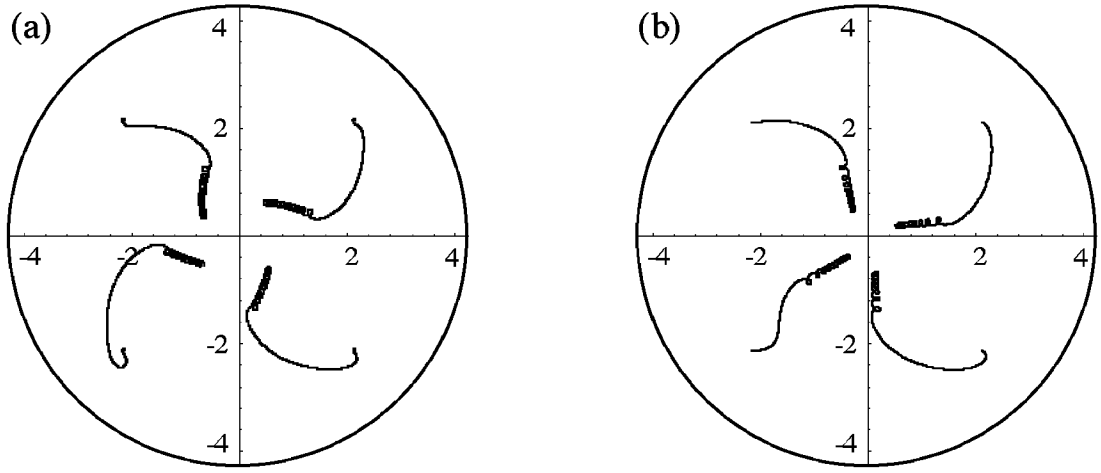

Figure 6: Chemotaxis control by: (a) network Γ_3, (b) first-order extracted rule. Initial conditions were the same as in Fig. 3b, but simulation time $T = 4$ minutes.

Networks Γ_1 and Γ_2 were optimized with $b_i \neq 0$ in (3.6). This led to rules for which $\Omega_{\text{bias}} \neq 0$. For both Γ_1 and Γ_2, this bias was important for producing oriented movement, since the zeroth-order term was small. To demonstrate the existence of a different strategy, we optimized (3.6) while holding $b_i = 0$. The constant expansion coefficients for two such networks, Γ_3 and Γ_4, are shown in Table 1. Figure 6a shows chemotaxis control by network Γ_3. As defined by the fitness function (4.2), the behavior is less optimal than that in Fig. 3b, but does exhibit oriented movement up the gradient and dwelling near the peak. Figure 6b shows the result of keeping all terms through first order in (5.10), for network Γ_3. The resulting tracks are nearly identical to those in Fig. 6a. Further investigation showed that keeping only the zeroth-order term, or only the first-order term, were inadequate to produce chemotaxis, and that the second-order term was unimportant in general. Since the sign of z_0 is opposite that of z_1, chemotaxis in this network arises from a competition between zeroth- and first-order terms. Thus Γ_3 also uses a combination of klinokinesis and klinotaxis, but unlike Γ_1 and Γ_2, here both terms are required. Network Γ_4 functions similarly to Γ_3, but with opposite handedness.

6 Discussion

We have shown that small, linear networks of graded-potential neurons are capable of controlling nematode-like chemotaxis. This suggests that the biological network need not rely heavily upon nonlinearities to produce chemotaxis behavior. The chemotaxis strategies identified here are candidate mechanisms for chemotaxis control occurring in *C. elegans* during runs. They are also candidate mechanisms for *C. elegans* thermotaxis (Hedgecock and Russell, 1975), since the control problem for this behavior is similar. Whether or not additional strategies are available using tumbles remains an open question.

Our model for nematode chemotaxis differs significantly from the kinetic model of Epstein *et al.* (1976) and the algorithmic model of Green (1976), since ours is based on a neural network. It therefore lays groundwork for understanding the neural control of chemotaxis in *C. elegans*. It differs from previous optimized network models of chemotaxis by Beer (1992), in that it is based specifically on nematode biomechanics and neuroanatomy. Our model differs from previous network models of both Beer (1992) and Ferrée *et al.* (1997), in that it is linear, and therefore analytically solvable.

Using analytical techniques from linear systems theory, we extracted computational rules that describe how these linear networks control chemotaxis. The major strength of this approach is that the network model (3.6), which depends on many parameters, could be replaced by a simple rule (5.10), which depends on only a few parameters. The convergence of the rule by first order makes intuitive sense, because as seen in (5.12), the first time derivative of the stimulus has a simple relation to the gradient $\vec{\nabla}C$, and chemotaxis is defined as oriented movement in a gradient (Dunn, 1990). The analysis identified two distinct computational strategies. In the first strategy, the dC/dt–term competes with a constant bias to produce oriented movement up the gradient. In the second strategy, the dC/dt–term competes with the C–term to produce similar behavior. These computational strategies are analogous to pure klinotaxis, and a combination of klinotaxis and klinokinesis, respectively, as defined by Dunn (1990). Our results, therefore, suggest seeking correlations between $d\theta/dt$ and dC/dt, and perhaps C, in behavioral data from real nematodes.

This approach should also be applicable to models of the *C. elegans* chemotaxis network that are more biologically realistic in several ways. First, the model could be made more realistic by including all neurons and synaptic connections present in the biological network. Because our approach is not based on the assumption of a particular number of neurons or pattern of synaptic connections, however, the analytical results will be identical provided that the network is linear. Second, the chemosensory current could be made to depend nonlinearly on the stimulus C, as is the case for many chemosensory neurons in other animal (Morales *al.*, 1994). For example, C in (3.4) could be replaced with $\ln C$. The network would still be linear in voltage, and the analytic solution would have the same form as (5.3), but with C replaced by $\ln C$. This would lead to a modified form of the computational rule (5.10), with C replaced by $\ln C$, dC/dt replaced by $(1/C)dC/dt$, etc. Third, the model could be generalized to include sensory adaptation, believed to be essential for some forms of chemotaxis (Fraenkel and Gunn, 1940, revised 1961). This could be introduced into the model by making κ_{sens} in (3.4) a dynamic variable. Because this would introduce a new

source of time dependence, but presumably not new voltage dependence, analytic solutions could still be obtained. An open question is whether changes of this sort lead to more effective chemotaxis control. Networks with nonlinear voltage dependence present a greater challenge. For nonlinear models which can be characterized by a finite Volterra series, however, a Taylor series expansion of the input, in each term of the Volterra series, may also lead to comprehensible rules for chemotaxis.

Acknowledgments

The authors thank C. I. Bargmann for providing unpublished data, and J. T. Pierce and T. M. Morse for helpful discussions. This work was supported by NIMH MH11373, NIMH MH51383, NSF IBN 9458102, ONR N00014-94-1-0642, the Sloan Foundation, and the Searle Scholars Program.

References

Bargmann, C. I. and H. R. Horvitz (1991). Chemosensory neurons with overlapping functions direct chemotaxis to multiple chemicals in *C. elegans*. *Neuron* 7: 729-742.

Beer, R. D. and J. C. Gallagher (1992). Evolving dynamical neural networks for adaptive behavior. *Adaptive Behavior* 1(1): 91-122.

Berg, H. C. and D. A. Brown (1972). Chemotaxis in *Escherichia coli* analyzed by three-dimensional tracking. *Nature* 239: 500-504.

Boyce, W. E. and R. C. DiPrima (1977). *Elementary differential equations and boundary value problems.* John Wiley & Sons, Inc.

Davis, R. E. and A. O. W. Stretton (1989). Signaling properties of *Ascaris* motor neurons: Graded active responses, graded synaptic transmission, and tonic transmitter release. *J. Neurosci.* 9: 415-425.

Dunn, G. A. (1990). Conceptual problems with kinesis and taxis. In: Armitage, J. P. and J. M. Lackie (Eds.) *Biology of the chemotactic response.* Cambridge University Press. pp. 1-13.

Dusenbery, D. B. (1976). Chemotactic behavior of mutants of the nematode *C. elegans* that are defective in their attraction to NaCl. *J. Exp. Zool.* 198: 343-352.

Dusenbery, D. B. (1980). Responses of the nematode *Caenorhabditis elegans* to controlled chemical stimulation. *J. Comp. Physiol. A* 136: 327-331.

Epstein, H. F., M. M. Isachsen and Edwin A. Suddleson (1976). Kinetics of movement of normal and mutant nematodes. *J. Comp. Physiol.* 110: 317-322.

Ferrée, T. C., B. A. Marcotte and S. R. Lockery (1997). Neural network models of chemotaxis in the nematode *Caenorhabditis elegans*. In: Mozer, M. C., M. I. Jordan and T. Petsche (Eds.) Advances in Neural Information Processing Systems 9. MIT Press. pp. 55-61.

Ferrée, T. C. and S. R. Lockery (1998). Chemotaxis control by linear recurrent networks. In: Bower, J. (Ed.) Computational Neuroscience: Trends in Research. Plenum Press.

Fraenkel, G. S. and D. L. Gunn (1940, revised 1961). The orientation of animals – kineses, taxes and compass reactions. Dover Press, New York.

Goodman, M. B., D. H. Hall, L. Avery and S. R. Lockery (1998). Active currents regulate sensitivity and dynamic range in *C. elegans* neurons. Submitted to *Neuron*.

Green, C. D. (1976). Simulation of nematode attraction to a point in a flat field. *Behaviour* LXI: 130-146.

Hedgecock, E. M. and R. L. Russell (1975). Normal and mutant thermotaxis in the nematode *Caenorhabditis elegans*. *Proc. Natl. Acad. Sci.* 72: 4061-4065.

Lewis, J. A. and J. A. Hodgkin (1977). Specific neuroanatomical changes in chemosensory mutants of the nematode *C. elegans*. *J. Comp. Neurol.* 172: 489-510.

Masters, T. (1995). Advanced algorithms for neural networks: A C++ sourcebook. John Wiley & Sons, Inc.

Morales, B., G. Ugarte, P. Labarca and J. Bacigalupo (1994). Inhibitory K^+ current activated by odorants in toad olfactory neurons. *Proc. R. Soc. Lond.* 257: 235-242.

Niebur, E. and P. Erdös (1991). Theory of the locomotion of nematodes: Dynamics of undulatory progression on a surface. *Biophys. J.* 60: 1132-1146.

Niebur, E. and P. Erdös (1993). Theory of the locomotion of nematodes: Control of the somatic motor neurons by interneurons. *Math. Biosci.* 118: 51-82.

Rogalski, T. M., B. D. Williams, G. P. Mullen and D. G. Moerman (1993). Products of the *unc*-52 gene in *Caenorhabditis elegans* are homologous to the core protein of the mammalian basement membrane heparan sulfate proteoglycan. *Genes Dev.* 7: 1471-1484.

Rutherford, T. A. and N. A. Croll (1979). Wave forms of *Caenorhabditis elegans* in a chem-

ical attractant and repellent and in thermal gradients. *J. Nematol.* 11(3): 232-240.

Toida, N., H. Kuriyama, N. Toshiro and Y. Ito (1975). Obliquely striated muscle. *Physiol. Rev.* 55: 700-756.

Van Houten, J. (1978). Two mechanisms of chemotaxis in *Paramecium. J. Comp. Physiol. A*, 127: 167-74.

Ward, S. (1973). Chemotaxis by the nematode *Caenorhabditis elegans*: Identification of attractants and analysis of the response by use of mutants. *Proc. Nat. Acad. Sci. USA* 70: 817-821.

Ward, S. (1978). Nematode chemotaxis and chemoreceptors. In: Hazelbauer, G. L. (Ed.) Taxis and behavior. Chapman and Hall, London. pp. 141-168.

Waterston, R. H., J. N. Thomson and S. Brenner (1980). Mutants with altered muscle structure in *Caenorhabditis elegans. Dev. Biol.* 77:271-302.

Waterston, R. H. (1988). Muscle. In: Wood, W. B. (Ed.) The nematode *Caenorhabditis elegans.* Cold Spring Harbor Laboratory Press. pp. 281-336.

Wicks, S. R., C. J. Roehrig and C. H. Rankin (1996). A dynamic network simulation of the nematode tap withdrawl circuit: Predictions concerning synaptic function using behavioral criteria. *J. Neurosci.* 16(12): 4017-4031.

White, J. G., E. Southgate, J. N. Thompson and S. Brenner (1986). The structure of the nervous system of *C. elegans. Phil. Trans. R. Soc. London* 314: 1-340.